CHAPTER IV

RESULTS AND DISCUSSION OF $GaAs_{1-x}N_x$ ALLOY BULK LAYERS

In this chapter, we describe optical and structural results of the high N-containing GaAsN film with N concentration (x) as high as x = 0.050. This N concentration is the highest N concentration, which can be grown. Since, the optical property of GaAsN film has been degraded with higher N incorporation. In order to improve the optical quality of this film, the effects of post-growth thermal annealing on structural and optical properties have also been studied.

4.1 Structural and Optical Investigation

In order to evaluate the N concentration in the GaAsN grown layer on the GaAs (001) substrate, it is the first required to know the lattice parameters of the epilayer perpendicular ($a_\perp$) and parallel ($a_{//}$) to the GaAs (001) surface, which are generally calculated from a symmetric (004) and an asymmetric (115) HRXRD, respectively. Figure 4.1 shows a (004) HRXRD $2\theta/\omega$ scan of the GaAsN layer on GaAs (001) substrate. The separation between the GaAs and GaAsN reflection peaks is estimated to be 1.448°, so the $a_\perp$ is determined to be 5.546 Å. In addition, Pendellösung fringes are clearly visible due to a finite thickness and abrupt interface between the layer and the substrate. The abrupt interface between the GaAs and GaAsN layer indicates that the as-grown GaAsN layer has in-plane lattice matched to the GaAs substrate without any defect, which is produced by misfit dislocation at the interface. Since the separation between the nearest fringes corresponds to a layer thickness. Using standard formula [37], thus, the thickness of GaAsN layer is calculated to be 157.0 nm.

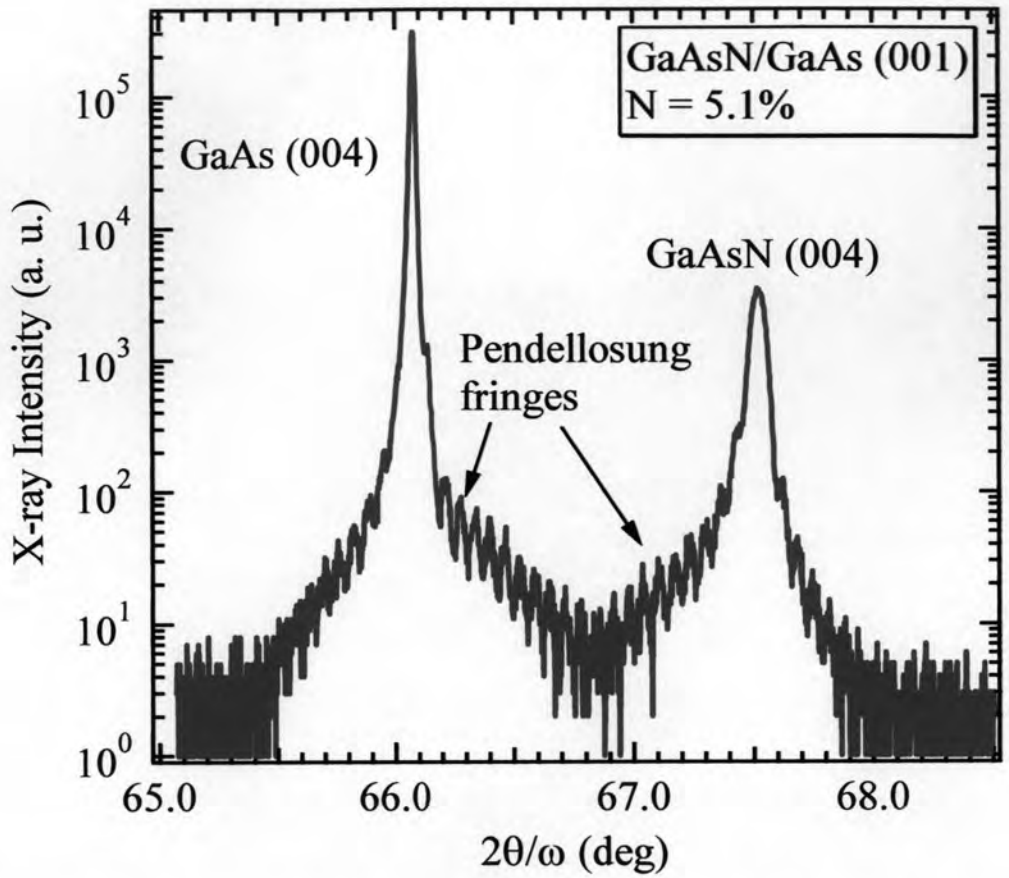

Figure 4.1: Symmetrical (004) HRXRD *2θ/ω* curve of the as-grown $GaAs_{0.949}N_{0.051}$ layer

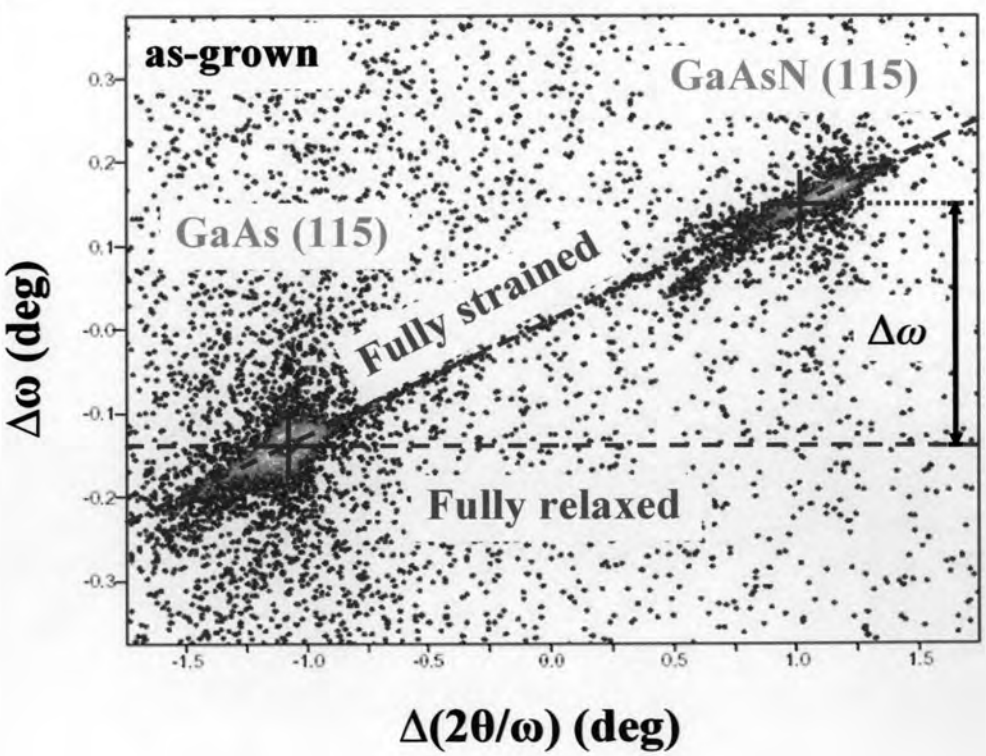

Figure 4.2: Asymmetric (115) reciprocal lattice map of the as-grown $GaAs_{0.949}N_{0.051}$ layer.

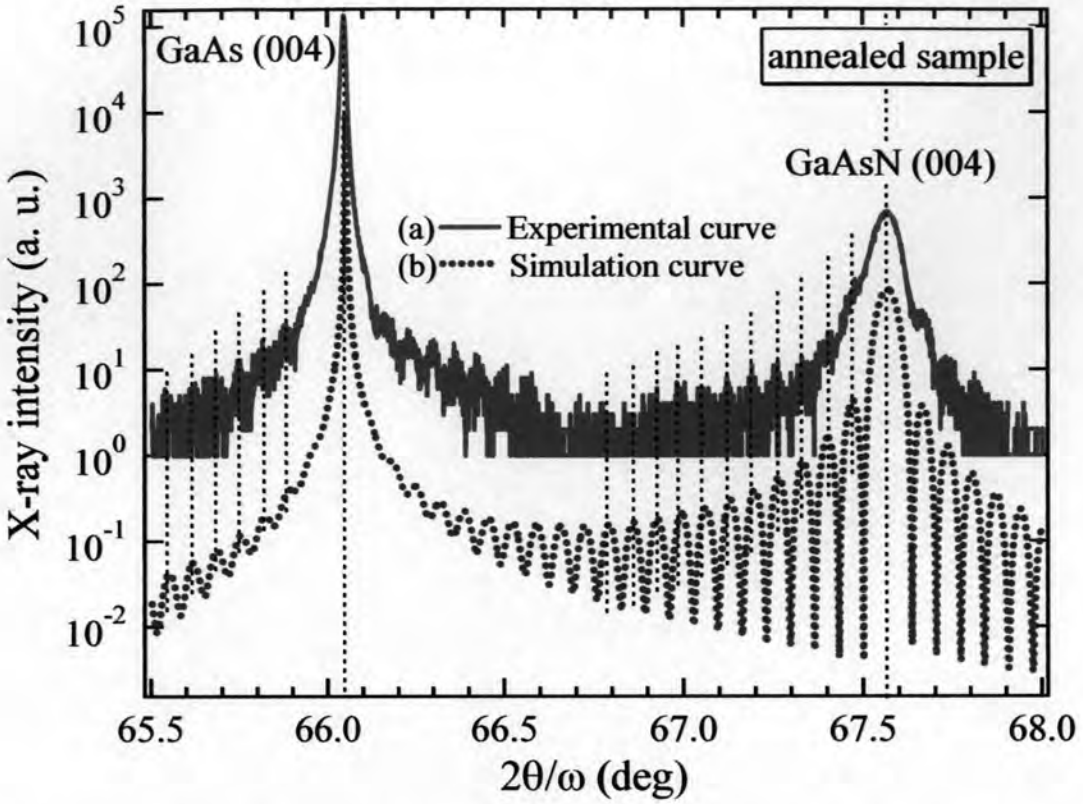

Figure 4.3: (004) XRD patterns of as-grown $GaAs_{0.949}N_{0.051}$ layer. The (a) solid curve is the experimental data and (b) the dashed curve is a simulated result using the dynamical-theory simulation software.

Figure 4.2 shows a reciprocal space map of the (115) reflection. It is clearly seen that the GaAsN peak is lying on the fully strained line. This indicates that the GaAsN layer is under coherently strained and exhibits a good epitaxial quality. Using both the (004) $2\theta/\omega$-scan and the (115) reciprocal space mapping measurements [38], $a_{//}$ is determined to be 5.653 Å. Note that this value is in an excellent agreement with the lattice constant of GaAs. Thus, the N concentration is estimated from the lattice parameters using Vegard's law (see in section 3.2) [38] to be 5.1%.

Another way that can determine the N concentration and layer thickness of the GaAsN layer is using the dynamical-theory simulation technique. In Fig. 4.3, the (004) $2\theta/\omega$-scan pattern of the GaAsN layer is fitted with the initial conditions using dynamical-theory simulation software. The initial conditions for the simulation consist of (i) strain in the GaAsN layer which is fully strained in our case, (ii) the N concentration used to adjust the GaAsN peak, and (iii) the layer thickness designed to

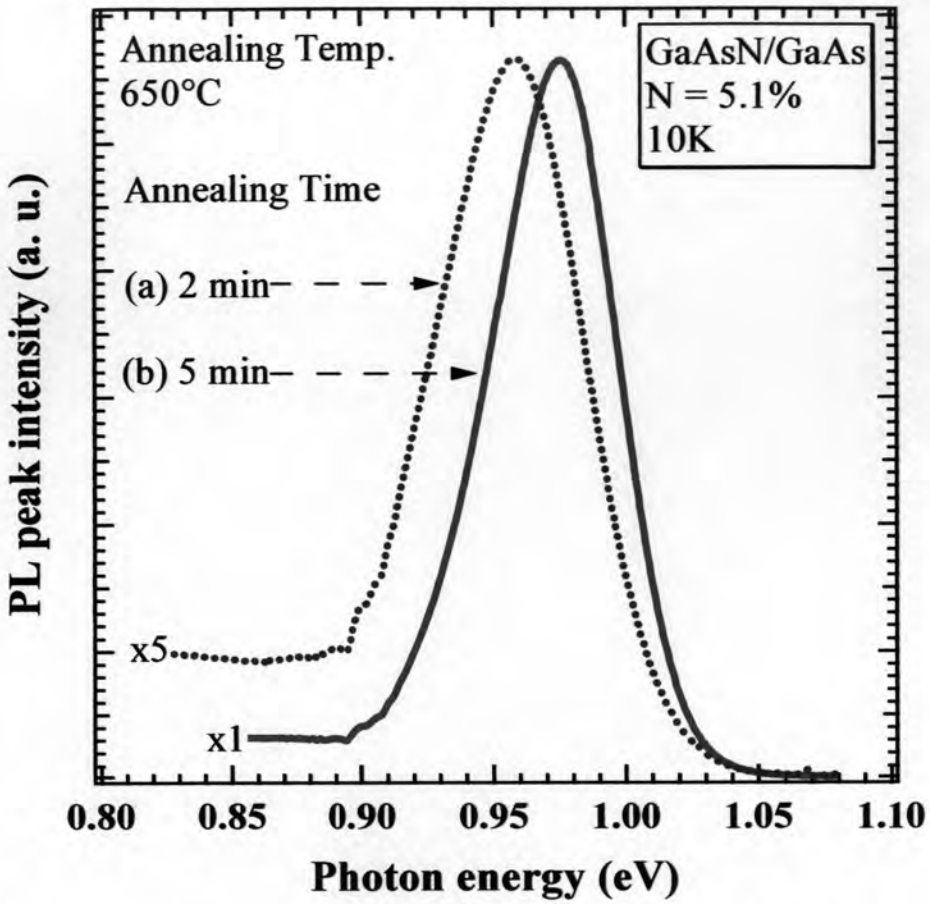

Figure 4.4: Low-temperature (10K) PL spectra of the annealed $GaAs_{0.949}N_{0.051}$ layers at 650°C for different annealing times; (a) 2 min and (b) 5 min.

fine-tune the separation between the Pendellösung fringes. The simulated curve (b) is found to agree with the experimental curve (a), as shown in Fig. 4.3. The N concentration and the layer thickness are estimated to be 5.1% and 157.0 nm. These results are consistent with the experimental values obtained from the HRXRD measurements. This suggests that the simulation method is also a reliable technique to determine the exact N concentration and layer thickness.

In order to observe the surface morphology of GaAsN layer, the optical microscopy image was performed, as shown in Fig. 4.8 (a). The surface morphology of the as-grown layer shows no surface cross-hatch patterns. This confirms that the as-grown layer is coherently grown on GaAs substrate and exhibits a good epitaxial quality. However, it is found that the luminescence signal cannot be detected from this as-grown GaAsN layer. This is due to a highly non-radiative recombination centers in such high N-containing samples [12, 13].

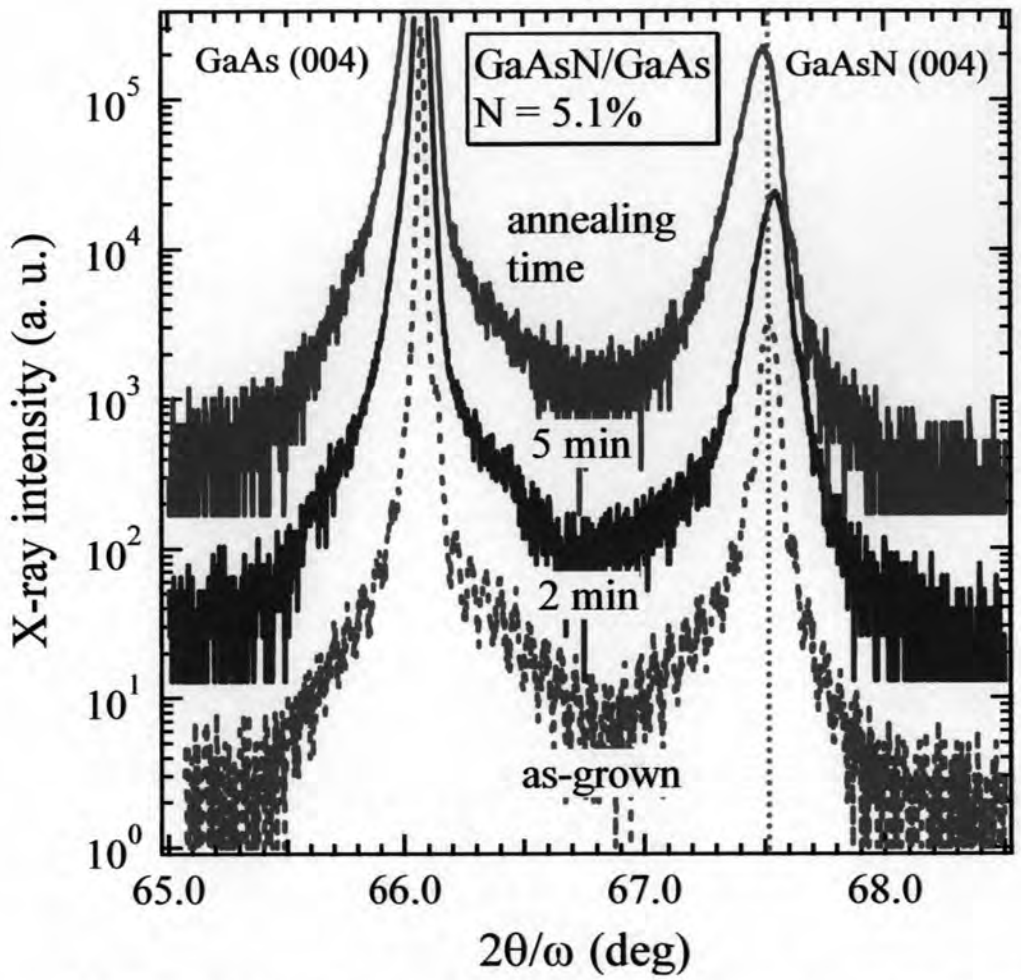

Figure 4.5: (004) HRXRD *2θ/ω* curves of the as-grown and annealed (650°C for 2 min and 5 min) $GaAs_{0.949}N_{0.051}$ layer.

4.2 Effects of Post-Growth Thermal Annealing on Optical Property

To improve the optical quality of as-grown GaAsN layer, the post-growth thermal annealing was performed. Figure 4.4 illustrates low-temperature (10K) PL spectra of the $GaAs_{0.949}N_{0.051}$ layer annealed at 650°C for annealing time of (a) 2 min and (b) 5 min. After annealing, the changes in the PL peak energy, the values of a full width at half maximum (FWHM) and the PL integrated intensity are clearly observed. Each PL spectrum is a single peak without any deep-level related luminescence and low-energy tail. This emission shows a substantial blue-shift with the longer annealing time, and the long wavelength emission at about 1.3 μm (0.95 eV) is observed for annealing time of 2 min. In general meaning, this blue-shift is attributed

mainly to three possible reasons: (i) the N out-diffusion; (ii) the strain relaxation in the GaAsN layer (see detail in section 2.1.2); and (iii) the improvement of alloy uniformity resulting in the decrease of the localization potential.

To clarify this point, we have taken the (004) HRXRD $2\theta/\omega$ profiles, the (115) reciprocal space mapping and the Raman spectra of the GaAsN layers before and after annealing. The changes in the N concentration resulting from annealing are determined firstly. Figure 4.5 shows the (004) HRXRD $2\theta/\omega$ curves of the GaAsN layers before and after annealing. For annealed layer, the FWHM of GaAsN (004) peak is increased with increasing annealing time. This increase in FWHM is attributed to non-uniformity of d-spacing in (004) plane resulting in the increasing of alloy non-uniformity and defect generation at the interface. Based on the PL result, the FWHM of PL peak is decreased resulting in the improvement of alloy uniformity. So the increasing of FWHM of GaAsN (004) peak can be attributed to defect generation at the interface. This defect generation is induced by the misfit dislocation. With increasing annealing time, disappearance of the Pendellösung fringes is clearly observed, indicating that the annealed layers show higher interfaces roughness. In addition, the 2 min annealing results in a shift of the GaAsN diffraction peak to a higher angle, indicating an increasing of N concentration. On the other hand, longer annealing time up to 5 min resulted in a shift of the GaAsN diffraction peak to a lower angle close to the substrate peak. This may come from a reduction of N concentration. Thus, with increasing annealing time from 2 to 5 min the GaAsN peak shifts to lower diffraction angle, this may be due to the decreasing of N concentration.

To make clear this point, the (115) reciprocal mapping measurement was also performed to determine the N concentration and strain state in annealed layer. Figure 4.6 shows the results of the (115) reciprocal space mapping of (a) the 2 min and (b) 5 min annealed samples. The GaAsN (115) peak is not at the fully strained line for both annealed samples. These results indicate that the residual strain in all the annealed layers is partially relaxed. A reduction of the residual strain is due to the strain relaxation of the lattice by an introduction of misfit dislocations. This result corresponds to the increase in FWHM of GaAsN (004) peak and the disappearance of the Pendellösung fringes for annealed layers. Since, the elliptic contours of GaAsN (115) peak, which indicates the layer bending due to the residual strain, is rotated for longer annealing times. The shape of GaAsN (115) diffraction points is considered

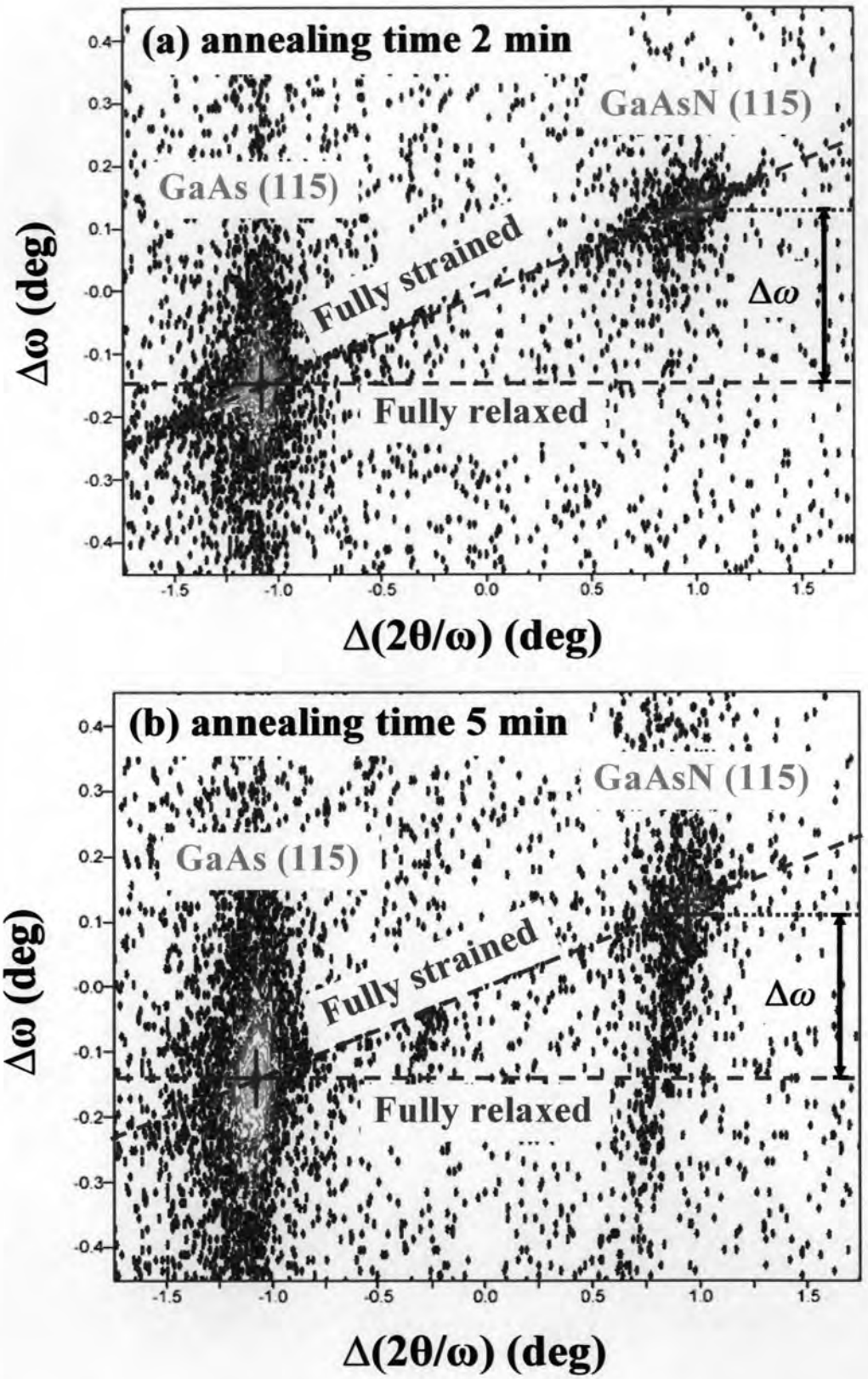

Figure 4.6: Reciprocal lattice maps of the (115) reflection of the $GaAs_{0.949}N_{0.051}$ layer annealed at 650°C for (a) 2 min and (b) 5 min.

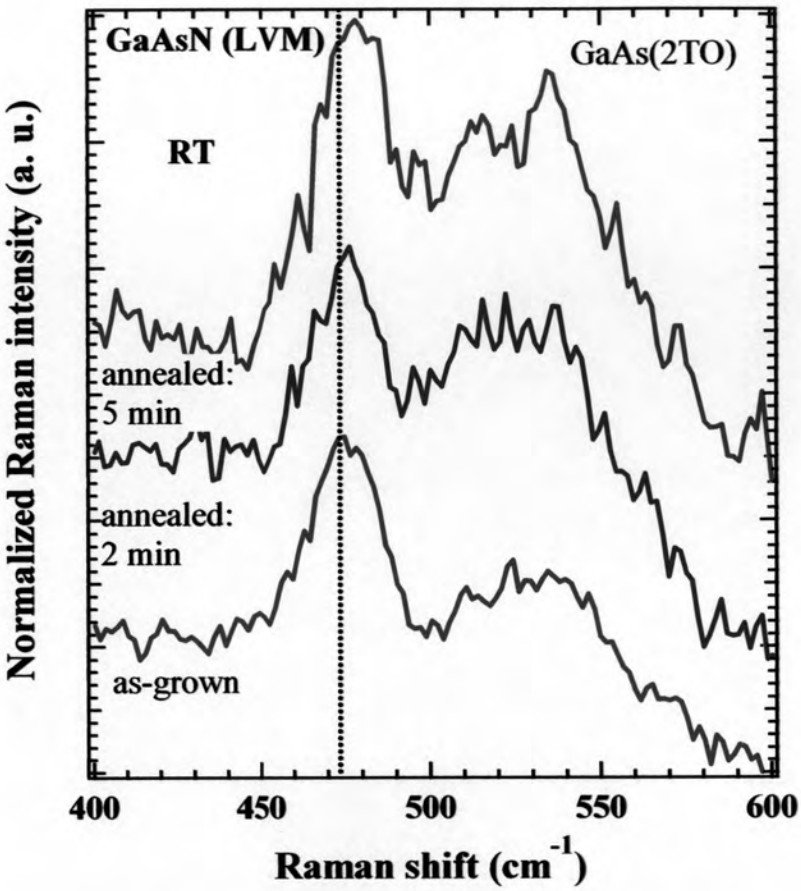

Figure 4.7: Raman spectra of the as-grown and annealed (at 650°C for 2 min and 5 min) $GaAs_{0.949}N_{0.051}$ layers.

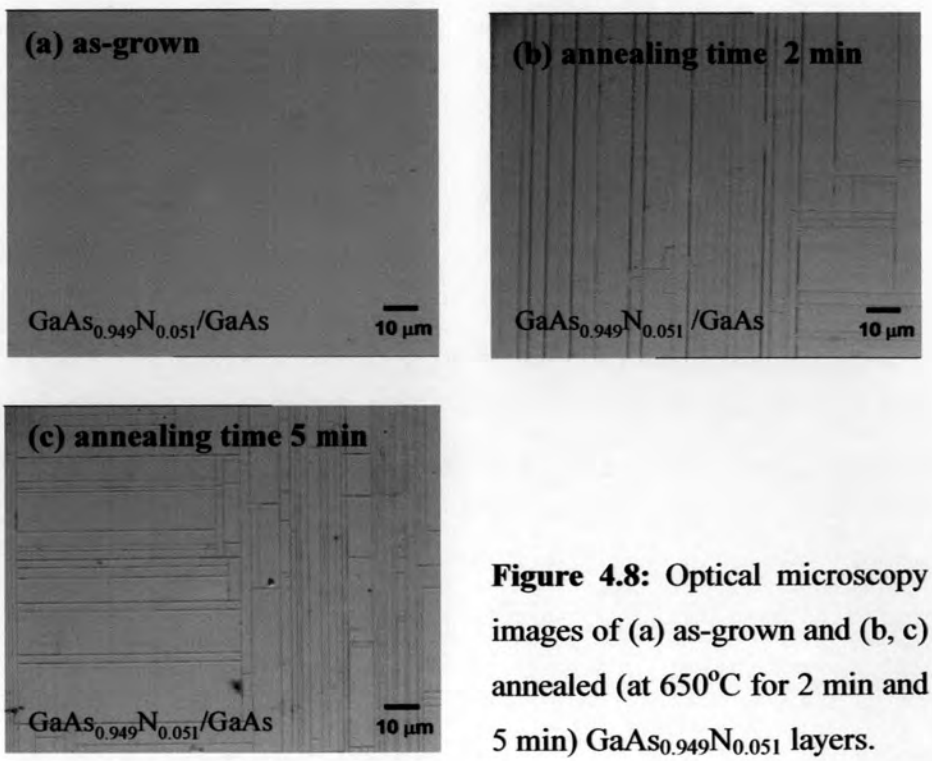

Figure 4.8: Optical microscopy images of (a) as-grown and (b, c) annealed (at 650°C for 2 min and 5 min) $GaAs_{0.949}N_{0.051}$ layers.

to be higher broad along ω-axis with increasing of annealing time. These results demonstrate an influence of the post-growth thermal annealing on an increase of the tensile strain, which will produces the strain relaxation in such high N-containing layer, to a critical point of structural qualities of the layer. In addition, broadening in ω-axis of GaAs peak is broader than that of GaAsN peak. This result suggests that the defect generation penetrates to the GaAs layer higher than that to the GaAsN layer due to the difference in bond strength between GaAs and GaN bond.

As shown in Fig. 4.6, the difference between the GaAs and GaAsN peaks along with ω-axis ($\Delta\omega$) for 2 and 5 min are estimated to be 0.280° and 0.257°, respectively. Thus, the $a_{//}$ are calculated to be 5.649 and 5.644 Å for annealing time 2 and 5 min, respectively, indicating the increasing of the in-plane lattice-mismatched from 0.07% to 0.16% with increasing of annealing time. From the values of $a_{\perp}$ and $a_{//}$ for annealing time 2 and 5 min, the N concentration are calculated to be 5.3% and 5.5%, respectively. It can be seen that the N concentration and strain relaxation increase with increasing annealing time.

The Raman scattering technique was also carried out in order to confirm the N concentration in GaAsN layer. It is also clearly seen in Fig. 4.7 that the normalized N-related local-vibrational mode (LVM) Raman intensity somewhat increases with an increasing of annealing time. Since, the integrated intensity of a Raman line is proportional to the number of corresponding oscillators [39]. Therefore, the integrated intensity of the N-related LVM in GaAsN is proportional to the N concentration in the layer. In addition, a gradual blue-shift of the N-related LVM Raman frequency is also observed. This strongly demonstrates an increase in the N content for longer annealing time. Hence, longer annealing up to 5 min did not result in N out-diffusion. But, it may be well-justified that the strain relaxation is occurred in the annealed layers.

The strain relaxation in the GaAsN layer after annealing can be examined by direct observation on surface morphology. The observation demonstrates the surface cross-hatch patterns of annealed layer, as indicated in Fig. 4.8. This result confirms that the strained relaxation is occurred in annealed layer. These observations are consistent with the (004) HRXRD $2\theta/\omega$ scan and the (115) reciprocal space mapping results. The increasing of the N concentration on lattice sites due to the interstitial N atoms generated in the growth process may replace the As atoms on the lattice sites to become more stable substitution N atoms through the thermal annealing process. This

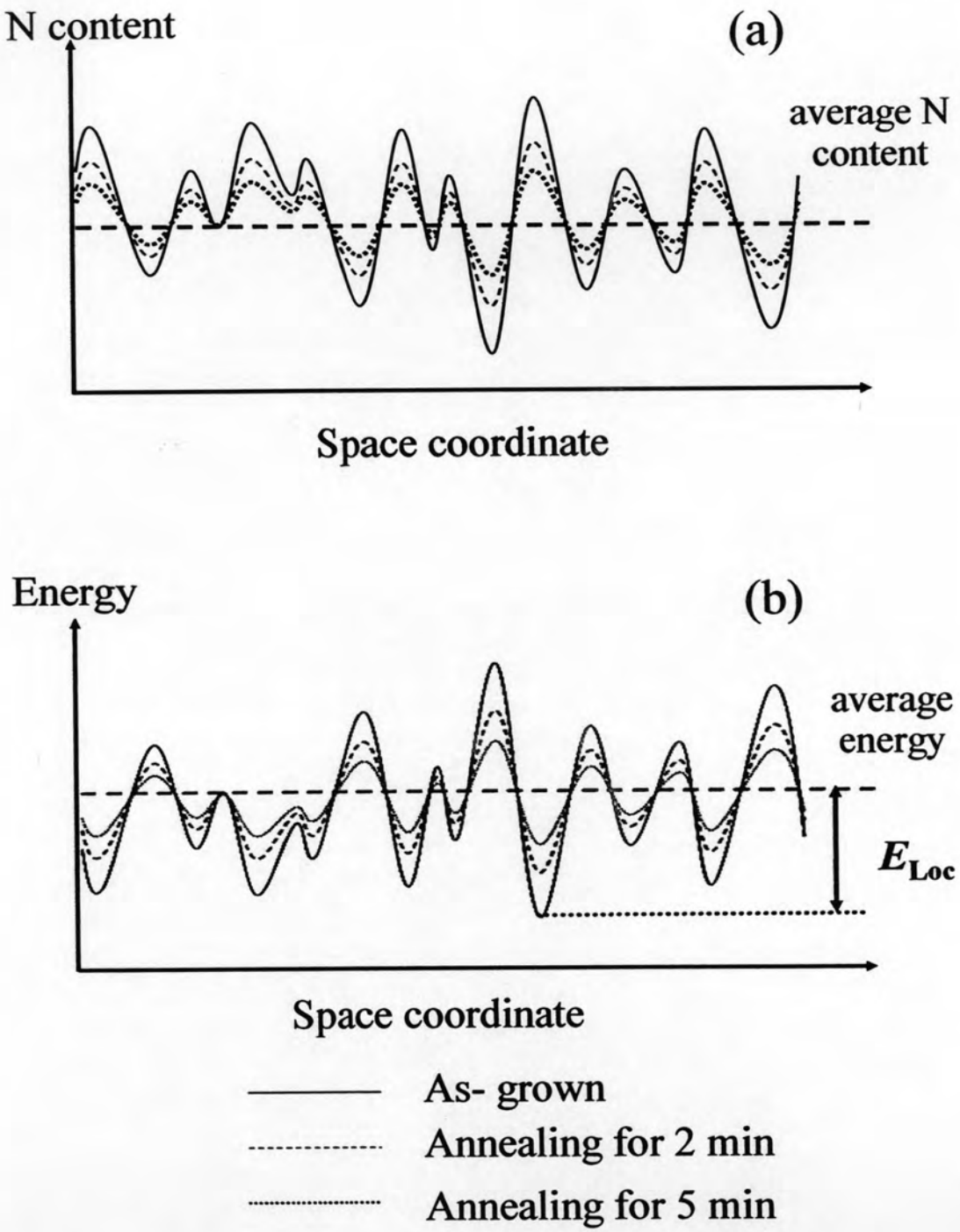

Figure 4.9: (a) The appearance of N composition fluctuations and their evolution as post-growth thermal annealing process, (b) also shown is the corresponding post-growth thermal annealing on potential fluctuation of the conduction band

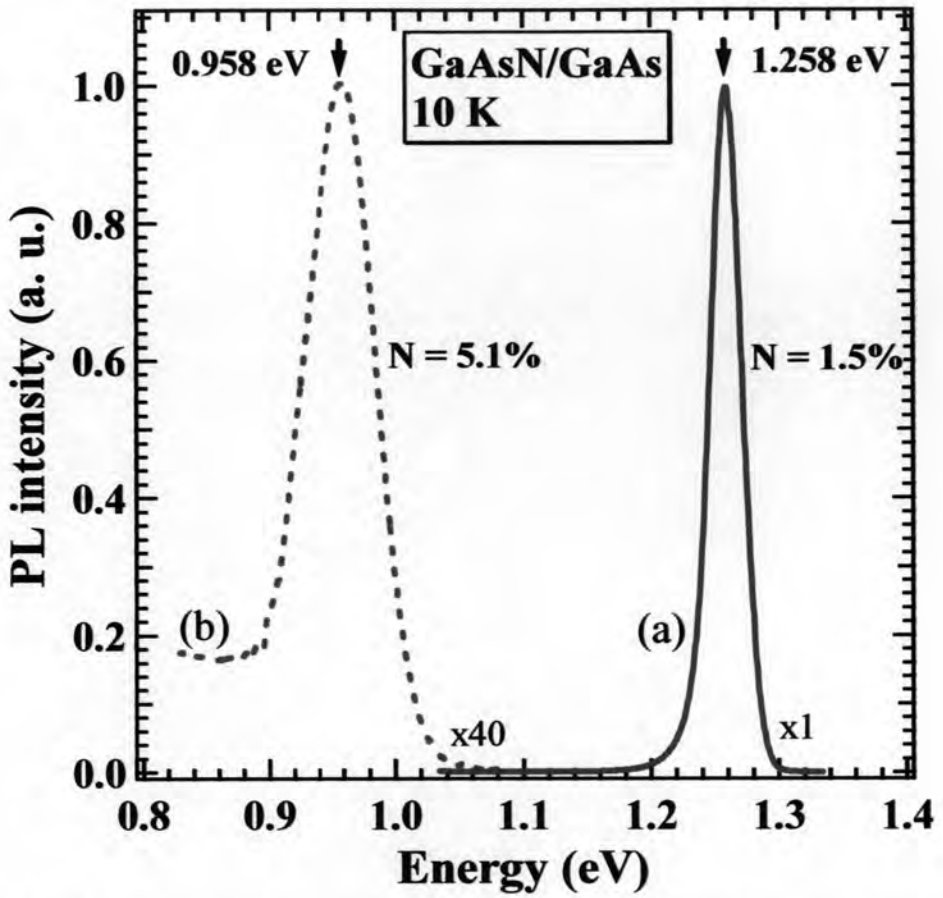

Figure 4.10: Low-temperature (10K) PL spectra of (a) as-grown $GaAs_{0.985}N_{0.015}$ and (b) annealed $GaAs_{0.949}N_{0.051}$ layers at 650°C for annealing time 2 min.

suggests that the high N-containing induced the reduction of critical thickness of GaAsN layer. Then, the initial layer thickness (157.0 nm) is higher than the critical thickness, thereby introducing strain relaxation in high N-containing layer. Furthermore, the diffusion of N atoms inside the layer homogenizes the initial N composition fluctuation in the as-grown alloy [40, 41]. Note that no indication of N out-diffusion is observable. Therefore, our results suggest that an improvement of composition uniformity and the strain relaxation in the GaAsN layer will account for the observed blue-shift in the PL peak energy after annealing. Based on the fact mentioned above, we will analyze how the post-growth thermal annealing affects on the nitrogen diffusion. The diagram of band-edge fluctuation for GaAsN due to distribution of N atoms and their evolution during annealing process are shown in Fig. 4.9. The conduction band edge fluctuations (solid line) and the effect of homogeneity induced by annealing process (dashed and dotted lines) are also shown in this figure.

To avoid the effects of thermal annealing treatment on strain relaxation in the high-N containing GaAsN layer, we can do two ways: (i) reduction of N concentration to decrease strain and mismatch between GaAsN film and GaAs substrate; (ii) reduction of layer thickness to be lower than the critical thickness.

4.3 Effects of N Incorporation on Optical Property

In order to clarify the effects of N concentration on the optical property of GaAsN alloy, the PL spectra of high and low N-containing GaAsN films are compared. Figure 4.10 shows the comparison of the PL spectra at low-temperature (10 K) between as-grown $GaAs_{0.985}N_{0.015}$ and annealed $GaAs_{0.949}N_{0.051}$ layers. The PL spectrum of as-grown $GaAs_{0.985}N_{0.015}$ layer in Fig. 4.10 (a) shows a single peak at 1.258 eV without any deep-level related luminescence at low energy tail. With increasing of N concentration, the PL spectrum of annealed $GaAs_{0.949}N_{0.051}$ layer (Fig. 4.10 (b)) also reveals a single peak with a large red-shift to be at 0.958 eV. Moreover, with increasing of N concentration, the increase in FWHM of PL peak and large reduction of PL peak intensity are clearly observed. It can be suggested that the increase in FWHM of PL peak is due to the increase in the alloy composition fluctuation. In addition, the large reduction of PL peak intensity with increasing the N concentration implies that the low PL efficiency is due to the increasing of the N-related non-rediative recombination centers. However, the informed optical property of GaAsN films from the low-temperature PL is not sufficient to know the transition energy states in GaAsN alloy. Thus, the temperature dependent PL will be analyzed, in the next section.

4.4 Temperature-dependent PL

In this section, we attempt to determine and deeply understand optical transition in GaAsN alloy. The temperature dependence of PL spectra is analyzed to understand the optical transition or transition energy states in GaAsN alloy. Figure 4.11 shows the temperature dependence of PL spectra for (a) as-grown $GaAs_{0.985}N_{0.015}$ and (b) annealed $GaAs_{0.949}N_{0.051}$ layers. The PL spectra were measured at temperature ranging from 10 K to 300 K. It can be seen that the PL peak intensity is rapidly

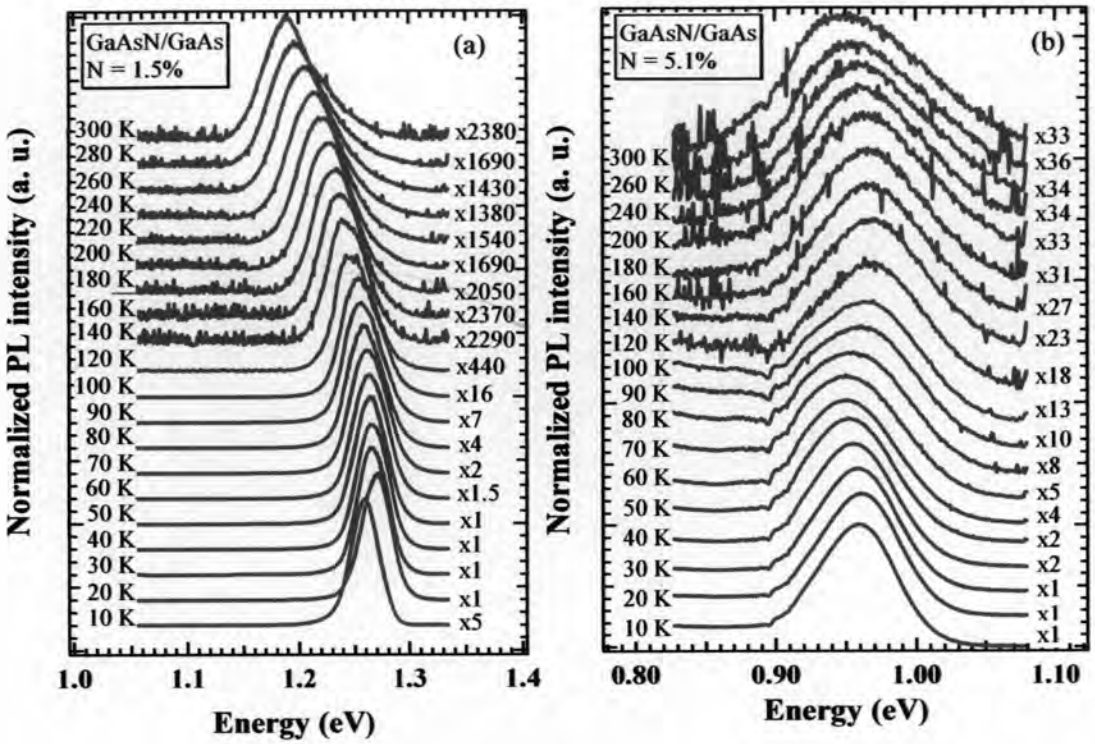

Figure 4.11: Temperature dependence of PL spectra for (a) as-grown $GaAs_{0.985}N_{0.015}$ and (b) annealed $GaAs_{0.949}N_{0.051}$ layers.

quenched with increasing temperature for both the $GaAs_{0.985}N_{0.015}$ and $GaAs_{0.949}N_{0.051}$ layers, indicating the present of non-radiative recombination centers in GaAsN alloys.

4.4.1 Temperature Dependence of PL Peak Position

The PL peak positions were evaluated by the best fit assuming the Gaussian curve. Figure 4.12 shows the temperature dependence of the PL peak position of (a) as-grown $GaAs_{0.985}N_{0.015}$ and (b) annealed $GaAs_{0.949}N_{0.051}$ layer. In order to understand the origin of the changes in PL peak position, we calculate the bandgap energy of GaAsN using the BAC model. Also, the evolution of temperature dependence of bandgap energy is estimated using the empirical Varshni model [42]. The PL peak position from the temperature dependence and the calculated bandgap energy from empirical Varshni model are compared to estimate the transition energy states in GaAsN layer. The solid lines in Fig. 4.12 represent the calculated bandgap

energy of $GaAs_{0.985}N_{0.015}$ and $GaAs_{0.949}N_{0.051}$ using the empirical Varshni model. By varying the temperature T, the bandgap energy is

$$E_g(T) = E_g(0) - \frac{\alpha T^2}{\beta + T}. \quad (4.1)$$

Where $E_g(T)$ and $E_g(0)$ are the bandgap energy of $GaAs_{1-x}N_x$ at temperature T and absolute zero, respectively. α and β are Varshni parameters. The values of α and β for $GaAs_{1-x}N_x$ alloy system is expected to obey Vergard's law, i. e., to be linearly dependence on the N concentration (x). For $GaAs_{0.985}N_{0.015}$ and $GaAs_{0.949}N_{0.051}$ alloys, the values of α and β can be determined using a linear interpolation between these values of GaAs and c-GaN. The values of α and β for GaAs and c-GaN as well as the values of α and β for $GaAs_{0.985}N_{0.015}$ and $GaAs_{0.949}N_{0.051}$ are summarized in Table 4.1. In order to determine $E_g(0)$ of $GaAs_{1-x}N_x$, the bandgap energy of $GaAs_{1-x}N_x$ at 300 K ($E_g(300)$) is calculated using band anticrossing (BAC) model (see section 2.1.2). The $E_g(300)$ of $GaAs_{0.985}N_{0.015}$ and $GaAs_{0.949}N_{0.051}$ alloys are calculated to be 1.188 and 0.917 eV, respectively. Taking these values for $E_g(300)$, the $E_g(0)$ each samples can be calculated using Eq. (4.1) and the calculated bandgap energy shown in Fig. 4.11 (a) for $GaAs_{0.985}N_{0.015}$ and (b) $GaAs_{0.949}N_{0.051}$ alloys.

In Fig. 4.12, in comparison between the PL peak position and calculated bandgap energy (solid line) shows that at low temperature, the PL peak position of $GaAs_{0.985}N_{0.015}$ and $GaAs_{0.949}N_{0.051}$ is not originated from bandgap energy of GaAsN alloy. This indicates that at low temperature, the carriers can be trapped by the localized states [15, 41, 42]. These localized states or the localization potential are

Table 4.1: Band structure parameters of GaAs, c-GaN and GaAsN alloys

parameters	GaAs	c-GaN	$GaAs_{0.985}N_{0.015}$	$GaAs_{0.949}N_{0.051}$
α ($\times 10^{-4}$ eV/K)	5.405 [43]	7.7 [36]	5.439	5.522
β (K)	204 [43]	600 [36]	210	224
E_g(0 K) (eV)	1.519 [43]	3.28 [36]	1.284	1.012
E_g(10K) (eV)	1.518	3.27	1.283	1.011
E_g(300K) (eV)	1.424 [43]	3.2 [36]	1.188	0.917

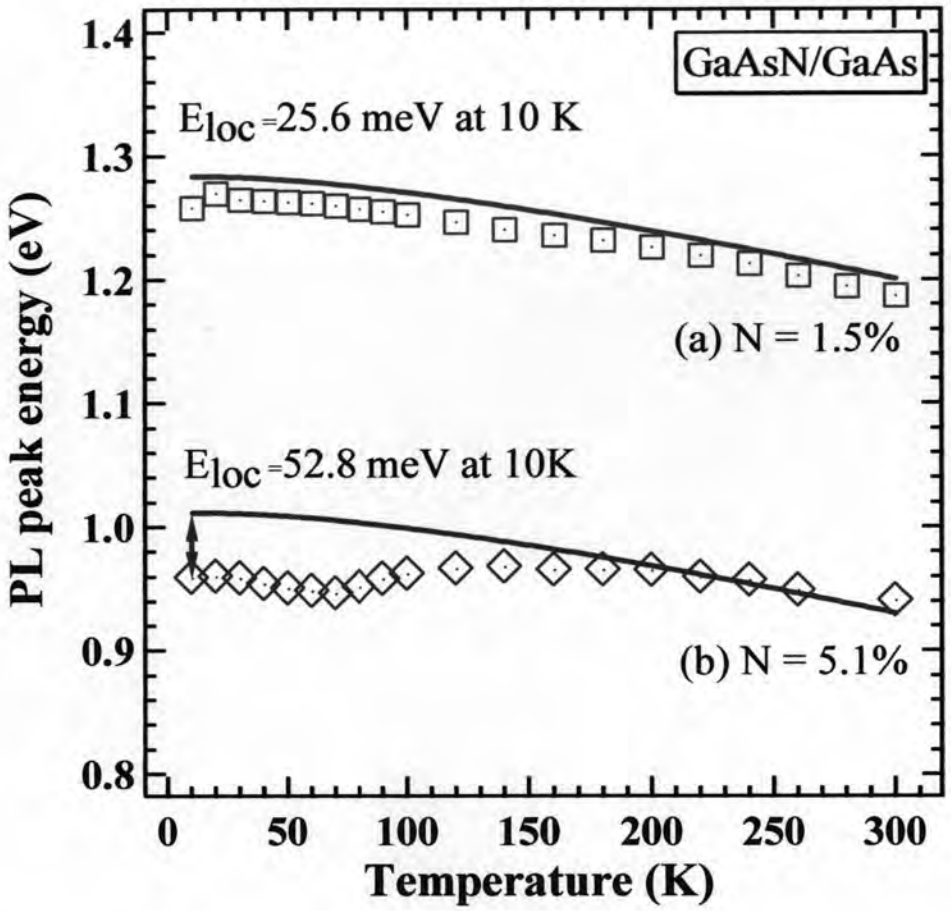

Figure 4.12: Temperature variation of PL peak energies for (a) as-grown $GaAs_{0.985}N_{0.015}$ and (b) annealed $GaAs_{0.949}N_{0.051}$ layers.

attributed to the conduction band edge fluctuation due to alloy composition fluctuation (see Fig. 4.9). The carriers localization energy at any temperature is given by the difference $E_{loc}(T) = E_g(T) - E_{PL}(T)$, where $E_g(T)$ is temperature dependence of bandgap energy and $E_{PL}(T)$ is temperature dependence of PL peak position. At the lowest temperature (T = 10 K), the localization energy is estimated to be 26.5 and 52.8 meV for $GaAs_{0.985}N_{0.015}$ and $GaAs_{0.949}N_{0.051}$ alloys, respectively, indicating that the localization energy is increased with increasing of N concentration. However, with increasing temperature, the PL peak position at high temperature is consistent with the bandgap energy of GaAsN alloy. As a result, the bandgap energy of $GaAs_{0.985}N_{0.015}$ and $GaAs_{0.949}N_{0.051}$ alloys at 300 K are estimated to be around 1.19 and 0.95 eV, respectively. The bandgap energy at 0.95 eV corresponds to a suitable the long-wavelength of 1.3 μm for optical communication systems operating at 300 K.

It is interesting to note that the temperature dependent PL of $GaAs_{0.985}N_{0.015}$ and $GaAs_{0.949}N_{0.051}$ alloys exhibit difference shape. In case of $GaAs_{0.985}N_{0.015}$ alloy, at the lowest temperature, the photo-generated carriers (or excitons), are trapped by the localized potential induced by alloy composition fluctuation, namely the fluctuation of conduction band edge. With increase of temperature from 10 K to 20 K, a small blue-shift appears because the excitons may be transferred to higher energy states. With further increasing of temperature, the reduction of PL peak position is clearly observed by a reason of the band-to-band transition. This strongly indicates that the PL peak position at high temperature is estimated to be the bandgap energy of $GaAs_{0.985}N_{0.015}$ alloy.

On the other hand, the temperature dependence of PL peak position of $GaAs_{0.949}N_{0.051}$ alloy in Fig. 4.12 (b) shows an S-shaped property. The increasing of temperature is an increase in the activation energy of carriers (or excitons), as a result, the carriers can move or hop to any energy states (see Fig. 4.14). With increase of temperature from 10 K to 70 K, a red-shift emerges as a result of the excitons gain sufficient thermal energy to rise above small potential barriers and thus is mobile to some range. In this case, some of these excitons may relax down and are trapped in the lower energy states where the recombination takes place. Therefore, the PL emission of higher energy states is suppressed and a red-shift occurs within the temperature range. However, with further increase in temperature from 70 K to 140 K, a blue-shift of PL peak position takes place. This blue-shift is attributed to the distribution of the localized exciton states close to the delocalized higher energy states. At higher temperature range (140 K < T < 300 K), the PL peak position is decreased according to the reduction of bandgap energy with increasing temperature. The relationship of temperature-dependent PL peak position of $GaAs_{0.985}N_{0.015}$ and $GaAs_{0.949}N_{0.051}$ shows that the localization potential increases with increasing of N concentration.

4.4.2 PL Peak Broadening in GaAsN Alloy

It is motivating to find the correlation between the temperature dependence of the PL linewidth as shown in Fig. 4.13 and those of PL peak energy as shown in Fig. 4.12. It can be seen that the N-shaped temperature dependence of the PL linewidth is

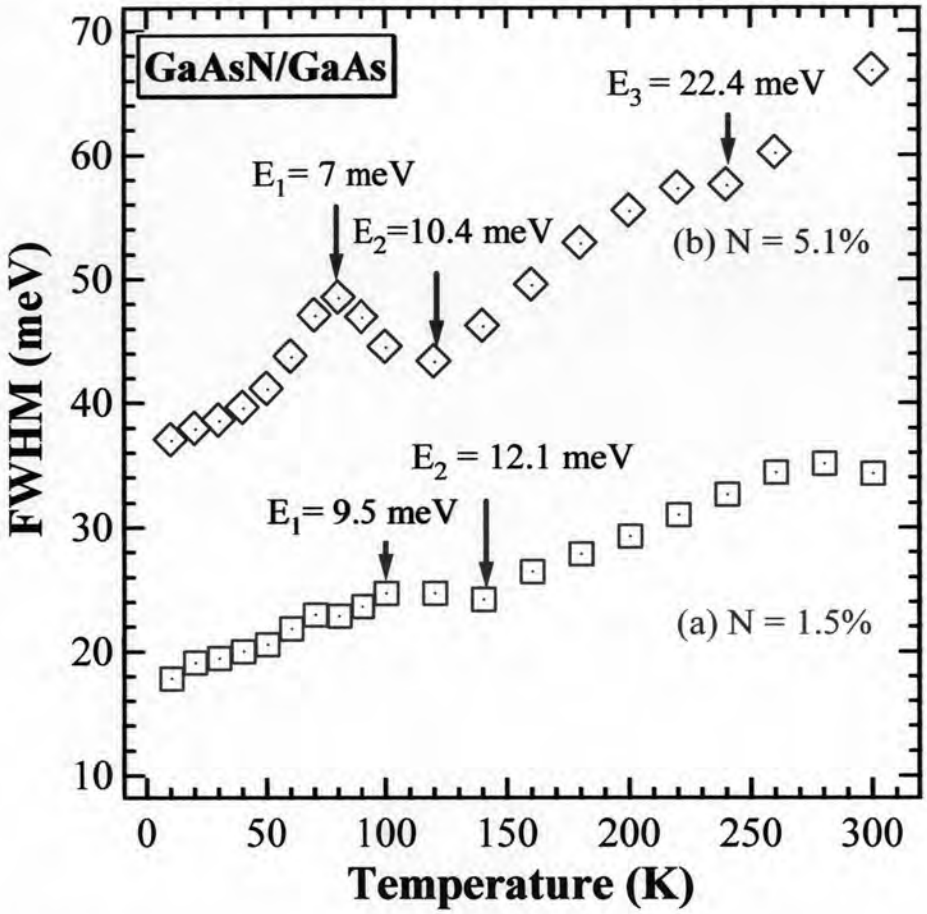

Figure 4.13: Evolution with the temperature of the full width at half maximum (FWHM) of PL peak for the (a) as-grown $GaAs_{0.985}N_{0.015}$ (b) annealed $GaAs_{0.949}N_{0.051}$ layers.

clearly observed for both $GaAs_{0.985}N_{0.015}$ and annealed $GaAs_{0.949}N_{0.051}$ layers. The FWHM of PL peak of higher N concentration sample is larger than those of lower N concentration sample observed for entire temperature. This phenomenon indicates the increasing degree of compositional and structural disorder with increasing N concentration. Generally, the spectral linewidth or FWHM linearly increases with temperature for band-to-band emission [42]. On the other hand, we observe the changes in PL linewidth for $GaAs_{0.985}N_{0.015}$ and annealed $GaAs_{0.949}N_{0.051}$ alloys, are so called N-shape property [42], indicating that the change of PL linewidth is due to localized states rather than band-to-band transition.

To explain the change of PL linewidth in GaAsN alloy, we will focus on the case of annealed $GaAs_{0.949}N_{0.051}$ layer. As the sample temperature is varied from 10 K

to 120 K, the PL linewidth is first increased and then decreased with temperature. This phenomenon suggests that competition between two distinct different energy states is occurred. With increase in temperature the carriers become mobile and two processes can occur; (i) the localized excitons become mobile across small potential to deeper localized states (PL red-shift), and (ii) the localized excitons become mobile across small potential and hop to higher energy states due to increasing of thermalization (PL blue-shift) (see Fig. 4.14 (b)). At 10 K < T < 80 K, while the temperature increases up to thermalization point (10 K < T < 80 K), some localized carriers become mobile and occupy shallower or deeper localized states at the same time, causing many difference of radiative recombination energy. This leads to an increase of PL linewidth. However, it is expected that the most localized carriers relax down to deeper localized states, corresponding to the red-shift of PL peak position. However, as the temperature is in the range of (80 K < T < 120 K), a decrease in FWHM is clearly observed. The narrowing of FWHM indicates that most carriers transfer to higher energy states, which corresponds to the blue-shift of PL peak position.

In addition, higher temperature range (120 K < T < 240 K), the PL linewidth is also increased and decreased again. This result can be explained in the same way as the temperature dependence of PL linewidth in the lower temperature range (10 K < T < 120 K). Further increase in temperature from 240 K to 300 K, thermal broadening of the carrier distribution occurs and the PL linewidth increases with increasing temperature, corresponding to band-to-band emission, which the PL linewidth usually depends linearly on temperature. Besides, the changing points of PL linewidth are estimated to be thermal activation energy, which activated the carriers across the potential barriers. The thermal activation energy is approximated using a thermal energy at each of changing point (see Fig. 4.13). The combination of thermal activation energy is estimated to be the localization energy of GaAsN alloy due to alloy composition fluctuation. For $GaAs_{0.985}N_{0.015}$ and $GaAs_{0.949}N_{0.051}$ alloys the localization energy are estimated to be 21.6 and 41.8 meV, respectively. These values are approximated equal to the value of localization energy from the difference between PL peak position and bandgap energy at 10 K. In the case of $GaAs_{0.985}N_{0.015}$ layer, the temperature dependence of PL linewidth can also be explained in the same approach as that of $GaAs_{0.949}N_{0.051}$ layer.

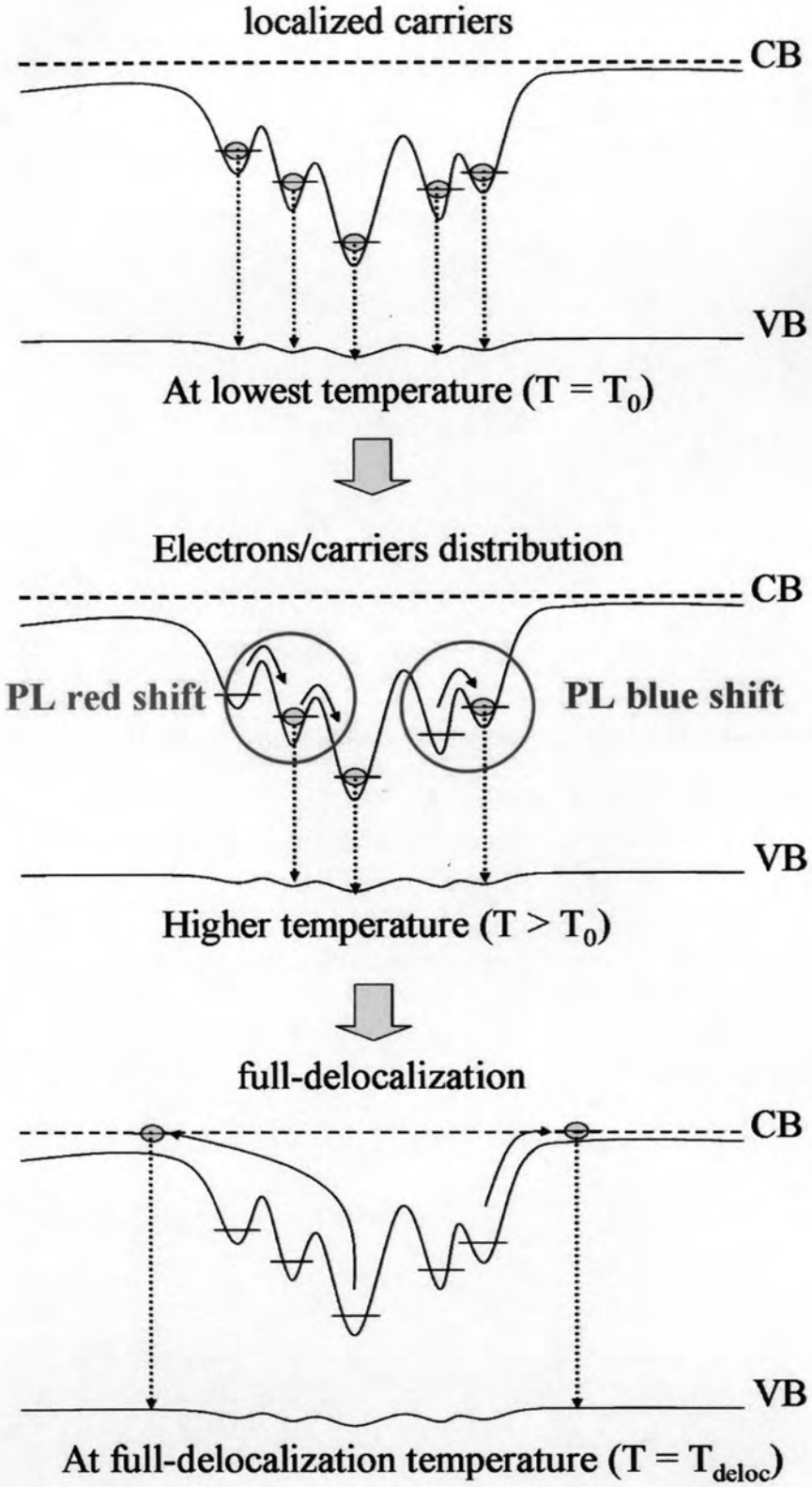

Figure 3.14: A schematic view of the transfer dynamics of localized carriers/excitons due to the local fluctuations of N concentration and their thermalization effect in GaAsN alloy.

4.5 Summary

The structural and optical properties of the high N-content $GaAs_{0.949}N_{0.051}$ layer were investigated. Our results showed the high quality strained GaAsN layer with high N up to 5.1% grown on GaAs (001) substrate by MOVPE. However, emission from the as-grown $GaAs_{0.949}N_{0.051}$ layer cannot be detected. After annealing, an improvement of PL intensity was clearly observed. PL spectrum with a near band edge excitonic emission without any deep-level related luminescence and low energy tail was confirmed. For annealing time at 2 min, the wavelength emission at about 1.3 μm (0.95 eV) was realized at 300 K. With the longer annealing times, the PL peak energy showed a substantial blue-shift. To make clear this point, the dependence of the annealing time on the N concentration was studied by HRXRD and Raman scattering measurements. The results demonstrated that, in such high N-containing layer, the PL blue-shift can be attributed to (i) an improvement of alloy uniformity and (ii) the strain relaxation. Besides, it is found that the optical transition is originated from the localized exciton states due to conduction band edge fluctuation resulting of alloy non-uniformity due to the N distribution. The localization energy in GaAsN alloy is increased with increasing of the N concentration.

Our results demonstrate that the N concentration as high as 5.1% is useful for optoelectronic devices such as laser diodes (LDs) emitting at 1.3 μm for optical communication systems.